Triggered polarization-entangled photon pairs from a single quantum dot up to 30 K

New Journal of Physics
The open–access journal for physics

Triggered polarization-entangled photon pairs from a single quantum dot up to 30 K

R Hafenbrak[1,4], S M Ulrich[1], P Michler[1], L Wang[2], A Rastelli[3] and O G Schmidt[3]

[1] Institut für Halbleiteroptik und Funktionelle Grenzflächen, Universität Stuttgart, Allmandring 3, 70569 Stuttgart, Germany
[2] Max-Planck-Institut für Festkörperforschung, Heisenbergstraße 1, 70569 Stuttgart, Germany
[3] Institute for Integrative Nanosciences, IFW Dresden, Helmholtzstraße 20, 01069 Dresden, Germany
E-mail: r.hafenbrak@ihfg.uni-stuttgart.de

New Journal of Physics **9** (2007) 315
Received 27 June 2007
Published 10 September 2007
Online at http://www.njp.org/
doi:10.1088/1367-2630/9/9/315

Abstract. The radiative biexciton–exciton decay in a semiconductor quantum dot (QD) has the potential of being a source of triggered polarization-entangled photon pairs. However, in most cases the anisotropy-induced exciton fine structure splitting destroys this entanglement. Here, we present measurements on improved QD structures, providing both significantly reduced inhomogeneous emission linewidths and near-zero fine structure splittings. A high-resolution detection technique is introduced which allows us to accurately determine the fine structure in the photoluminescence emission and therefore select appropriate QDs for quantum state tomography. We were able to verify the conditions of entangled or classically correlated photon pairs in full consistence with observed fine structure properties. Furthermore, we demonstrate reliable polarization-entanglement for elevated temperatures up to 30 K. The fidelity of the maximally entangled state decreases only a little from 72% at 4 K to 68% at 30 K. This is especially encouraging for future implementations in practical devices.

[4] Author to whom any correspondence should be addressed.

PII: S1367-2630(07)53775-4

Contents

1. Introduction

Triggered entangled photon pair sources are considered to be one of the most important resources in view of quantum information technology applications [1]. While most existing sources for entangled photons rely on nonlinear optical effects [2]–[5], triggered entangled photons provide the benefit of being event-ready for application. Such a source has been proposed [6] and recently demonstrated [7, 8].

After triggered optical excitation of two electron–hole pairs (biexciton $= |XX\rangle$) in a quantum dot (QD), the system provides a natural cascaded two-photon process. In a first step, the biexciton decays into one of the two possible optically active single-exciton states (one electron and one hole $= |X\rangle$) by emitting an XX photon, followed by an excitonic decay to the empty dot state by emitting a second X photon with typically somewhat different energy [9]. As is schematically shown in figure 1(a), the polarizations of the two photons are determined by the intermediate $|X\rangle$ exciton states which are typically split in energy due to electron–hole exchange interaction and QD confining potential anisotropy [10]. If this fine structure splitting ΔE_{FS} is much larger than the radiative linewidth ΔE_{rad} (see left panel), the two possible decay paths are distinguishable which results in the emission of classically polarization-correlated photon pairs [11]–[13]. By spectrally selecting only the overlap of the two polarization components, photon entanglement has been achieved [14], however on the account of significant signal losses. If the splitting is smaller than the radiative linewidth (figure 1(a) right panel), the two decay paths are indistinguishable, producing two vertically (horizontally) polarized entangled photons closely related to the situation in single atoms [15]. Two important prerequisites have to be fulfilled for a safe selection of adequate QDs whose fine-structure splittings ΔE_{FS} are either by nature or by an external tuning process smaller than the radiative linewidth (here: $\Delta E_{\mathrm{rad}} \sim 0.7\,\mu$eV). Firstly, the detection set-up should be clearly capable of spectrally resolving this regime. Secondly, the actually observed inhomogeneously broadened emission linewidth ΔE_{FWHM} due to spectral diffusion should be as small as possible. Both aspects have been realized in the current work. The spectral resolution of the micro-photoluminescence (μ-PL) set-up has been enhanced to $\sim$0.3 μeV (see section 2), and we fabricated QDs with inhomogeneous linewidths smaller than $\sim$10 μeV for pump powers near the exciton saturation power. This is a substantial improvement (factor of ~ 5) in comparison to previous reports on quantum dot-based entangled photon sources [7, 14] and an important step towards a reliable selection process which is necessary for technological applications.

2. Experiment

The sample considered here is grown by molecular beam epitaxy on semi-insulating GaAs (001) substrate. (In,Ga)As QDs with low surface density are obtained by growth of InAs at a substrate temperature of 500 °C. As described in [16], the QD emission is tuned in the sensitivity range of our Si detectors by overgrowing the QDs with 1.5 nm GaAs, followed by 4 min annealing (2 min at substrate temperature ramping from 500 to 560 °C plus 2 min at 560 °C) before continuing the growth of the GaAs cap layer. In order to improve the collection efficiency, QDs are embedded in the middle of a 260 nm GaAs layer (lambda-cavity) placed on top of 15 pairs of AlAs/GaAs (78.4/65 nm thick) and below a single pair of GaAs/AlAs. μ-PL measurements on individual QD structures are performed in a variable temperature helium-flow cryostat ($T = 4$ to 320 K) in combination with a confocal microscope assembly. One microscope objective (NA = 0.5) is used to focus the exciting laser on the sample surface (spot diameter $\sim$1.5 μm) and to collect the emerging luminescence. For non-resonant pulsed excitation of single (In,Ga)As/GaAs QDs above the GaAs barrier, a mode-locked Ti : sapphire laser with $\Delta t_{\text{pulse}} \approx 1.4$ ps wide pulses at a repetition rate of $f_{\text{laser}} = 76.2$ MHz is used. Alternatively, a stabilized cw-Ti : sapphire ring laser serves to continuously pump the sample in the case of sensitive high-resolution μ-PL experiments (see description below). Spectral dispersion and detection of the μ-PL signal is achieved by a computerized grating spectrometer equipped with an ℓN_2-cooled CCD camera for time-integration.

Especially for detailed investigations on the linewidth and/or fine structure of the emission from individual QDs, a high-resolution set-up has been implemented. In previous work, interferometric measuring techniques have been applied to resolve linewidth and polarization splitting from single QDs by inserting a Michelson interferometer in the detection path of a standard μ-PL set-up [17, 18]. Here, we use a scanning Fabry-Perot interferometer instead, providing the benefit of an even faster measurement of the fine structure splitting directly in the frequency domain. Based on the above described confocal μ-PL set-up, a periodically scanning Fabry-Perot-type interferometer (FPI) in conjunction with a sensitive avalanche photo diode (APD) for photon detection is connected to the auxiliary output port of a $f = 500$ mm (1200 ℓ mm^{-1}) spectrometer/monochromator unit. In this configuration, the monochromator (resolution $\Delta E_{\text{res}} = 50\,\mu$eV) is used to spectrally pre-select individual PL emission lines of interest which are subsequently fine-filtered by the FPI. Spectral fine scans over one or two free spectral ranges (FSR = 15 GHz or 62.035 μeV) by periodical variation of the mirror spacing d_{FPI} result in a repetitive series of resonances where the conditions of internal constructive interference enable mth order transmission at the selected wavelength according to $m \cdot \lambda = 2\,n\,d_{\text{FPI}}$. In this notation, $n = 1$ (air) denotes the refractive index of the medium between the FPI plates. For a controlled periodic tuning of the FPI resonance, a high-voltage ramp bias (0 to 1000 V) is applied to the piezo-electric etalon spacer elements by a stabilized external signal synthesizer. A necessary synchronization between the ramp generator bias sweeps and the detection loops of a multi-channel scaler (MCS) is accomplished through a logic 'start' trigger, thus allowing repetitive accumulations of the APD count rate as a function of the FPI tuning. Extensive tests of the high-resolution photoluminescence (HRPL) set-up have confirmed a significantly improved spectral resolution limit of $\Delta E_{\text{res}}^{\text{HRPL}} \approx 0.3\,\mu$eV, i.e. by a factor of $\sim$100 in comparison with the bare spectrometer assembly. A direct monitoring and/or selection of certain QD emission fine structure components is possible by a combination of a rotatable $\lambda/2$ zero-order wave plate followed by a fixed linear polarizer in front of the monochromator.

Investigations on two-photon correlations have been performed in terms of second-order $g^{(2)}(\tau)$ cross-correlation measurements on a Hanbury Brown and Twiss (HBT)-type set-up [19]. For these correlations, the collimated μ-PL signal from the sample is first divided into two orthogonal detection arms by a non-polarising 50%–50% beam splitter. Each arm is equipped with a tunable grating spectrometer ($1200\,\ell\,\mathrm{mm}^{-1}$) which acts as a monochromator to individually filter either the biexcitonic or the excitonic emission. For detection of single photons along the filtered channels, each monochromator is followed by a high-sensitivity APD with ultra-low dark noise (25 to 80 cts s^{-1} typ.). The recording of photon coincidence events is performed by a two-step process of time-amplitude conversion (TAC) and subsequent multi-channel analysis (MCA). For this, the TTL-shaped APD output pulses from each individual photon detection event serve as the 'start' (XX) and 'stop' (X) trigger channels of the TAC which converts the delay $\tau = t_{\mathrm{stop}} - t_{\mathrm{start}}$ within each photon pair into an equivalent bias pulse being detected by the MCA. The temporal resolution of this HBT set-up is $\Delta t_{\mathrm{res}}^{\mathrm{HBT}} = 600$ ps.

For a detailed analysis of the two-photon cascades by polarization-resolved cross-correlations in quantum state tomography (QST), rotatable $\lambda/2$ and $\lambda/4$ retarder plates in combination with 50%−50% polarising beam splitters have been introduced into the beam paths in front of each spectrometer. By a total of 16 combinations of polarization detection in accordance with the QST experiment and analysis scheme [20, 21], the two-photon density matrix $\hat{\rho}$ can be reconstructed from the Poisson-normalized $\tau = 0$ values of the corresponding $g^{(2)}_{XX,X}(\tau)$ traces. From the resulting representation of $\hat{\rho}$, conclusions about the degree of polarization entanglement can be derived in comparison with the expected scenarios of theory. Moreover, a classification of the achieved (classical or mixed entangled) photon polarization states in terms of fidelity F [22], concurrence C [23], tangle T and negativity N [24] can be derived.

3. Measurement results

The pre-selection of appropriate (In,Ga)As QDs has been performed as in previous work [7], i.e. QDs with emission energies around 1.40–1.42 eV have been chosen due to their minimal fine structure splitting [8, 25]. Figure 1(b) shows a characteristic, nearly background-free μ-PL spectrum of a single dot. The emission lines correspond to the radiative decay of excitonic $|X\rangle$, biexcitonic $|XX\rangle$ and charged excitonic $|X^{\star}\rangle$ carrier complexes. The observed emission lines are non-polarized, and no splitting is detected within the spectral resolution ($\Delta E_{\mathrm{res}}^{\mu\text{-PL}} \approx 50\,\mu$eV) of the μ-PL set-up.

In order to resolve the fine structure splitting ΔE_{FS}, polarization-dependent high-resolution μ-PL measurements with $\Delta E_{\mathrm{res}}^{\mathrm{HRPL}} = 0.3\,\mu$eV have been performed. Figure 2 shows the excitonic recombination lines of two QDs (QD A and QD B) exhibiting similar μ-PL spectra as discussed in figure 1(b). Under these high-resolution conditions, distinct differences become observable under different polarization configurations. The actual inhomogeneous linewidth of both dots is in the range of $\Delta E_{\mathrm{FWHM}} \approx 10\,\mu$eV, and QD A reveals a clear fine-structure splitting $\Delta E_{\mathrm{FS}} = 14.0 \pm 0.3\,\mu$eV under stepwise variation of the linear polarization detection angle. As here ΔE_{FS} is larger than the radiative homogeneous linewidth ($\Delta E_{\mathrm{rad}} \sim 0.7\,\mu$eV), both orthogonally polarized decay paths (see figure 1(a), left panel) can be distinguished, thus resulting in classically polarization-correlated photons. In contrast, QD B reveals an almost vanishing fine structure of $\Delta E_{\mathrm{FS}} = 0 \pm 0.3\,\mu$eV. As will be discussed later, QST measurements demonstrate a high degree of photon entanglement in the emission of this QD.

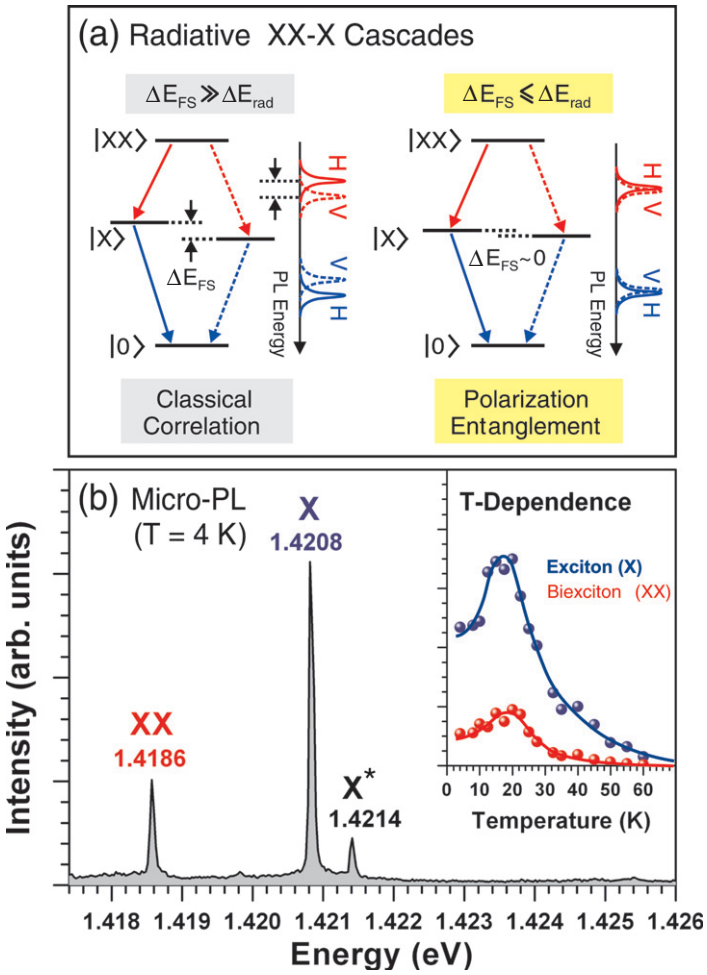

Figure 1. (a) Schematic representation of the cascaded radiative biexciton–exciton decay and the PL emission spectra: a fine structure splitting $\Delta E_{\mathrm{FS}} \gg \Delta E_{\mathrm{rad}}$ (left-hand side) much larger than the radiative emission line width manifests in distinguishable and therefore classically linear polarization-correlated photon pairs. In the regime of $\Delta E_{\mathrm{FS}} \leqslant \Delta E_{\mathrm{rad}}$ (right-hand side), the cascade paths become indistinguishable, thus creating path entanglement of collinearly polarized photon pairs. (b) Low-temperature ($T = 4\,\mathrm{K}$) μ-PL spectra of a single (In,Ga)As/GaAs QD under non-resonant pulsed optical excitation above the GaAs barrier: the observed distinct μ-PL signatures correspond to the channels of spontaneous radiative decay from excitonic $|X\rangle \rightarrow |0\rangle$, biexcitonic $|XX\rangle \rightarrow |X\rangle$, or charged excitonic $|X^{-}\rangle \rightarrow |\mathrm{e}^{-}\rangle$ ($|X^{+}\rangle \rightarrow |\mathrm{h}^{+}\rangle$) carrier configurations inside the QD, respectively. Inset: integrated μ-PL intensities of the excitonic and biexcitonic transitions as a function of temperature.

For practical implementations, e.g. under electrical injection conditions, the dots will be exposed to higher temperatures ($T > 10\,\mathrm{K}$) due to ohmic heating in a p-i-n diode-like structure. Therefore, a detailed knowledge of the temperature behaviour is indispensable for future applications. Systematic temperature-dependent μ-PL measurements have been performed, and

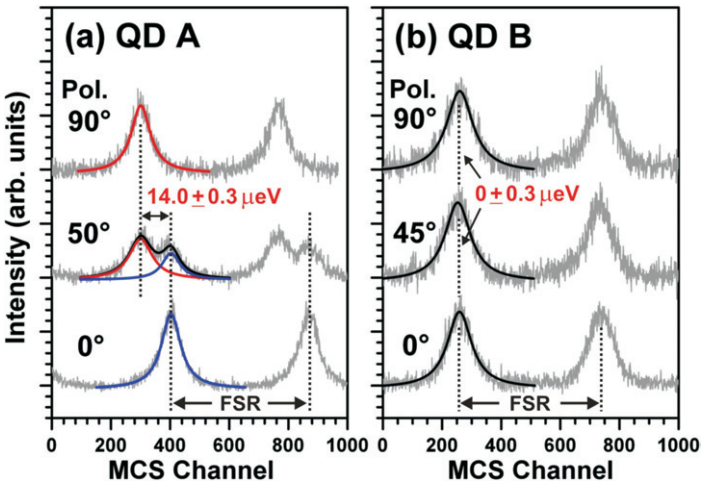

Figure 2. HRPL series of the excitonic recombination of two different QDs: each individual HRPL trace (vertically shifted for enhanced clarity) represents a spectral μ-PL scan of the filtered $|X\rangle \rightarrow |0\rangle$ decay channel over more than one full period of the interferometer's FSR (FSR $= 62.035\,\mu$eV), showing as two subsequent orders of transmission resonances. (a) Under variation of the linear polarization detection angle of 'QD A', a clear exciton emission fine structure with an energetic splitting of $\Delta E_{\mathrm{FS}} = 14.0 \pm 0.3\,\mu$eV is observable, whereas 'QD B' shows no splitting.

the inset graph of figure 1(b) depicts the spectrally integrated intensities of the excitonic and biexcitonic decay channels as a function of T. With increasing temperature, a distinct increase of the PL signal is observed for both emission lines up to a maximum value at $T \sim 18$ K, followed by strong decrease of the signal until almost no signal is observed above $T = 60$ K. The initial increase of quantum efficiency is indicative for a temperature-induced activation of 'frozen' carriers from shallow trap centres in the surrounding GaAs barrier matrix and/or faster carrier relaxation processes in this temperature regime. On the other hand, the decrease of the quantum efficiency beyond the former temperature range is caused by thermal emission of carriers (= losses) into the wetting layer. The early onset of thermal emission processes is due to the low carrier confinement energies of these type of QDs with nearly zero fine-structure splitting.

In order to gain detailed insight into the two-photon states, polarization-resolved $g^{(2)}_{XX-X}(\tau)$ second-order photon cross-correlation measurement series [19] have been performed. In figure 3, examples for the corresponding correlation traces as revealed in the linear and circular detection bases are depicted. As becomes evident from the linear basis results in figures 3(a) and (b), a high probability of collinearly polarized XX–X photon sequences following the same excitation cycle is reflected by a strong photon 'bunching', i.e. super-Poissonian statistics with an enhancement of $C_{VV} = 3.45 \pm 0.02$ as compared to uncorrelated light ($C_{\mathrm{Poisson}} = 1$). In contrast, the sequential emission of biexcitonic and excitonic photons under orthogonal linear polarization is significantly suppressed to a (normalized) value of $C_{\mathrm{VH}} = 0.41 \pm 0.02$. From the $\tau = 0$ correlation values in traces (a) and (b), a high collinear polarization correlation [8] of $\eta_{\mathrm{VV-VH}} = (C_{\mathrm{VV}} - C_{\mathrm{VH}})/(C_{\mathrm{VV}} + C_{\mathrm{VH}}) = 0.79 \pm 0.01$ can be derived.

In addition to measurements in the linear polarization basis, figures 3(c) and (d) show representative data from cross-correlations in co-circular ($R_{XX}R_X$) and contra-circular ($R_{XX}L_X$) configuration. As a remarkable result, a strong contra-circular 'bunching' signal is found

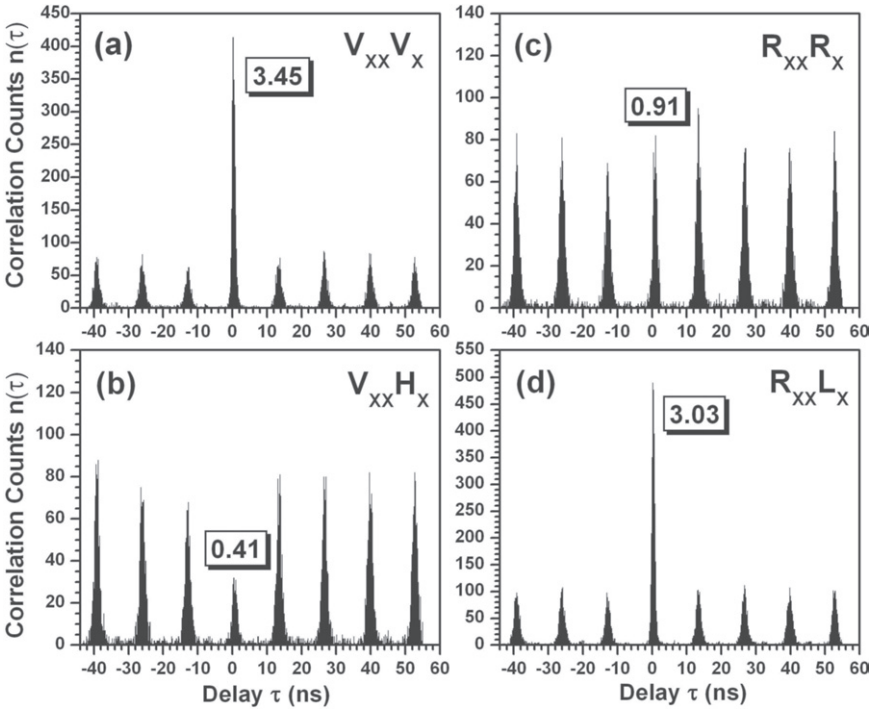

Figure 3. (a)–(d) Examples of polarization-dependent $g^{(2)}_{XX-X}(\tau)$ photon cross-correlation measurements in QST (16 combinations in total, after [20]). The traces were observed from the cascaded $|XX\rangle \rightarrow |X\rangle \rightarrow |0\rangle$ spontaneous radiative recombination between the biexcitonic and excitonic states of 'QD B' (see figure 1) under pulsed excitation. The applied polarization detection settings for biexciton (index XX) and exciton decay (index X) are sequentially labelled as vertical **V** (horizontal **H**) in the *linear* and right-handed **R** (left-handed **L**) in the circular basis, respectively. Numbers represent the Poisson-normalized integrals C of the central zero-delay correlation peaks with respect to uncorrelated photon coincidences at multiples of the laser repetition period $\Delta t_{\text{laser}} = f^{-1}_{\text{laser}} = 13.12$ ns.

($C_{\text{RL}} = 3.03 \pm 0.02$), whereas no such tendency appears under co-polarized detection. From these configurations, again a high degree of polarization correlation $\eta_{\text{RR-RL}} = (C_{\text{RR}} - C_{\text{RL}})/(C_{\text{RR}} + C_{\text{RL}}) = -0.54 \pm 0.01$ is evaluated, which is expected for entangled photon emission.

In order to derive the full information on the observed two-photon states, QST [20, 21] has been performed to derive the corresponding two-photon density matrices $\hat{\rho}$ in both cases. From an application of the QST scheme, the correspondingly calculated density matrices of photon emission from QD A as well as QD B are composed in figures 4(a) and (b), respectively, where $\hat{\rho}$ is represented by its real and imaginary parts, $\text{Re}(\hat{\rho})$ and $\text{Im}(\hat{\rho})$.

Beginning with the results obtained at $T = 4$ K from QD A, significant contributions appear only for the outer on-diagonal matrix elements of the real part which is in conformity with the expected behaviour of classical photon polarization–correlation. The additional observation of minor matrix contributions from orthogonal linear polarization (represented by the inner-diagonal elements $\leqslant 0.1$ of $\text{Re}(\hat{\rho})$) could be attributed to (i) the detection of uncorrelated

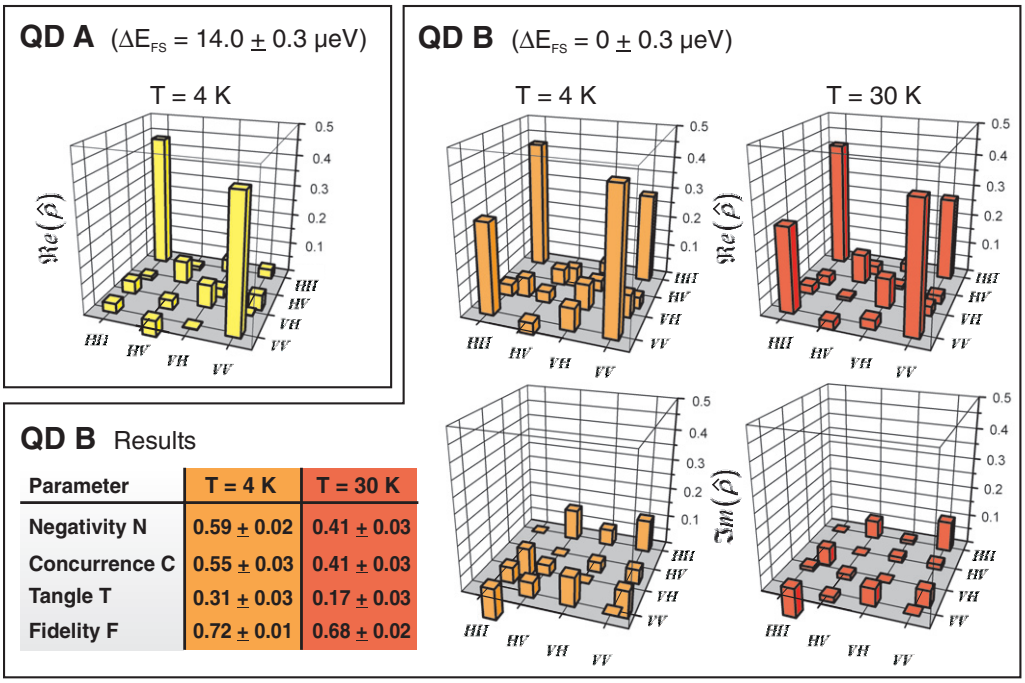

QD B Results

Parameter	T = 4 K	T = 30 K
Negativity N	0.59 ± 0.02	0.41 ± 0.03
Concurrence C	0.55 ± 0.03	0.41 ± 0.03
Tangle T	0.31 ± 0.03	0.17 ± 0.03
Fidelity F	0.72 ± 0.01	0.68 ± 0.02

Figure 4. QST of the two-photon density matrix: Reconstructed two-photon state density matrices (with $\mathrm{Re}(\hat{\rho})$, $\mathrm{Im}(\hat{\rho})$ as the real and imaginary parts) of the cascaded biexciton–exciton decay from a QD (QD A with resolvable fine structure splitting $\Delta E_{\mathrm{FS}} = 14.0 \pm 0.3\,\mu$eV, see figure 2(a)) and a second dot with degenerate exciton states (QD B with $\Delta E_{\mathrm{FS}} = 0 \pm 0.3\,\mu$eV). For QD A, the lifted exciton state degeneracy reflects in polarization-correlated XX-X photon sequences, which prohibit quantum entanglement due to distinguishability of photon pairs by energy and polarization. In contrast to QD A, the matrix of QD B reveals distinct off-diagonal elements and therefore strong indications of photon-path entanglement, as is also quantified by the parameters negativity $N \gg 0$, concurrence $C \gg 0$, $T = C^2 \gg 0$ and fidelity $F > 0.5$.

background photon events along the XX and X channels, and (ii) spin-flip processes between the intermediate excitonic fine structure levels, resulting in the known effect of recombination path intermixing [11]–[13].

In clear contrast to the former scenario, the real part of the density matrix obtained for QD B ($T = 4\,\mathrm{K}$) contains also strong outer off-diagonal elements with a magnitude of ∼0.3. This is a clear signature of the coherence between $V_{XX}V_X$ and $H_{XX}H_X$. Minor phase shifts between the above collinear polarization states are represented by the small ($\leqslant 0.1$) off-diagonal elements in $\mathrm{Im}(\hat{\rho})$. Different tests for entanglement according to literature are all positive for this QD (see table in figure 4). The obtained photon pair polarization state $\hat{\rho}$ emitted by QD B projects on to the entangled Bell state $|\Phi^+\rangle = (|H_{XX}H_X\rangle + |V_{XX}V_X\rangle)/\sqrt{2}$ with a large fidelity of $F = 0.72 \pm 0.01 (T = 4\,\mathrm{K})$.

With special consideration of photon entanglement, QST on QD B has been performed for further temperatures up to $T = 30\,\mathrm{K}$. Up to this temperature regime, intense enough PL emission signatures from biexcitonic and excitonic recombination could be observed (see inset of figure 1(b)). The reconstructed two-photon density matrix components $\mathrm{Re}(\hat{\rho})$ and $\mathrm{Im}(\hat{\rho})$

derived at 30 K are shown in the right panel of figure 4. Surprisingly, an almost identical matrix representation with similar magnitude of elements is found, which confirms a high degree of photon entanglement (see table in figure 4). The minor increase of the inner diagonal element from 0.09 at 4 K to 0.11 at 30 K indicates a slight spin decoherence of the intermediate exciton state. The projection of the measured state on to the Bell state $|\Phi^+\rangle$ reveals a high fidelity of $F = 0.68 \pm 0.02$.

Therefore, our results indicate the potential of semiconductor QDs for triggered entangled photon generation at elevated temperatures. Combined with recent advances in external tuning possibilities of the excitonic fine-structure, e.g. by electric-field [26, 27], strain [28], post-growth thermal treatment [29, 30] or magnetic field [7], QDs with higher confinement energies could be used which would consequently allow higher operation temperatures than the currently used QDs which exhibit low carrier confinement. Such improvements could lead to the realization of electrically-pumped triggered entangled photon sources.

4. Summary

In this paper, we presented a detailed investigation of non-classical light emission from single semiconductor QDs with special emphasis on photon pair entanglement. A high-resolution detection technique was introduced, allowing us to accurately and swiftly measure the fine structure of QDs with a resolution of $\Delta E_{\mathrm{res}} = 0.3\,\mu$eV. Polarization-dependent second-order cross-correlation measurements were performed, indicating classical polarization correlations between the two photons from the QD's biexciton–exciton decay. Choosing QDs of different fine structure splittings, we were also able to unambiguously distinguish the conditions of either classical correlation or entanglement by measuring the density matrix of the corresponding two-photon polarization states. We have found high polarization entanglement in the case of small fine structure and no entanglement for dots with large fine structure splitting at $T = 4$ K. From QST measurements performed at elevated temperatures up to 30 K, triggered entangled photon pairs could be verified. Over the full temperature range investigated, the projection fidelity of the two-photon polarization state on the maximally entangled bell state decreases only slightly from 72% at 4 K to 68% at 30 K. Our results suggest that operation above 30 K could be possible which would be important for electrical injection of carriers due to unavoidable ohmic heating in the structure. Therefore, a compact electrically-pumped semiconductor source of triggered polarization-entangled photon pairs seems to be feasible in the future.

Acknowledgments

We thank Harald Weinfurter for valuable discussions and gratefully acknowledge financial support from the DFG research groups 'Quantum optics in semiconductor nanostructures' and 'Positioning of single nanostructures—single quantum devices'.

References

[1] Bouwmeester D, Ekert A K and Zeilinger A 2000 *The Physics of Quantum Information* (Berlin: Springer)
[2] Shih Y H and Alley C O 1988 *Phys. Rev. Lett.* **61** 2921–4
[3] Kiess T E, Shih Y H, Sergienko A V and Alley C O 1993 *Phys. Rev. Lett.* **71** 3893–7
[4] Kwiat P G, Mattle K, Weinfurter H and Zeilinger A 1995 *Phys. Rev. Lett.* **75** 4337–41

[5] Edamatsu K, Oohata G, Shimizu R and Itoh T 2004 *Nature* **431** 167–70
[6] Benson O, Santori C, Pelton M and Yamamoto Y 2000 *Phys. Rev. Lett.* **84** 2513–6
[7] Stevenson R M, Young R J, Atkinson P, Cooper K, Ritchie D A and Shields A J 2006 *Nature* **439** 179–82
[8] Young R J, Stevenson R M, Atkinson P, Cooper K, Ritchie D A and Shields A J 2006 *New J. Phys.* **8** 29
[9] Moreau E *et al* 2001 *Phys. Rev. Lett.* **87** 183601–4
[10] Gammon D, Snow E S, Shanabrook B V, Katzer D S and Park D 1996 *Phys. Rev. Lett.* **76** 3005–8
[11] Santori C, Fattal D, Pelton M, Solomon G S and Yamamoto Y 2002 *Phys. Rev.* B **66** 045308
[12] Stevenson R M, Thomson R M, Shields A J, Farrer I, Kardynal B E, Ritchie D A and Pepper M 2002 *Phys. Rev.* B **66** 081302
[13] Ulrich S M, Strauf S, Michler P, Bacher G and Forchel A 2003 *Appl. Phys. Lett.* **83** 1848–50
[14] Akopian N, Lindner N H, Poem E, Berlatzky Y, Avron J and Gershoni D 2006 *Phys. Rev. Lett.* **96** 130501
[15] Aspect A, Grangier P and Roger G 1982 *Phys. Rev. Lett.* **49** 91–4
[16] Wang L, Rastelli A and Schmidt O G 2006 *J. Appl. Phys.* **100** 064313
[17] Kammerer C, Cassabois G, Voisin C, Perrin M, Delalande C, Roussignol P and Gérard J M 2002 *Appl. Phys. Lett.* **81** 2737–9
[18] Zwiller V, Aichele T and Benson O 2004 *Phys. Rev.* B **69** 165307
[19] Hanbury Brown R and Twiss R Q 1956 *Nature* **177** 27–9
[20] James D F V, Kwiat P G, Munro W J and White A G 2001 *Phys. Rev.* A **64** 052312
[21] Altepeter J B, Jeffrey E R and Kwiat P G 2005 Photonic state tomography *Advances in Atomic, Molecular, and Optical Physics* ed L Berman (Amsterdam: Elsevier)
[22] Jozsa R 1994 *J. Mod. Opt.* **41** 2315–23
[23] Hill S and Wootters W K 1997 *Phys. Rev. Lett.* **78** 5022–5
[24] Vidal G and Werner G F 2002 *Phys. Rev.* A **65** 032314
[25] Young R J, Stevenson R M, Shields A J, Atkinson P, Cooper K, Ritchie D A, Groom K M, Tartakovskii A I and Skolnick M S 2005 *Phys. Rev.* B **72** 113305
[26] Kowalik K, Krebs O, Lemaître A, Laurent S, Senellart P, Voisin P and Gaj J A 2005 *Appl. Phys. Lett.* **86** 041907
[27] Gerardot B D *et al* 2007 *Appl. Phys. Lett.* **90** 041101
[28] Seidl S, Kroner M, Högele A, Karrai K, Warburton R J, Badolato A and Petroff P M 2006 *Appl. Phys. Lett.* **88** 203113
[29] Seguin R *et al* 2006 *Appl. Phys. Lett.* **89** 263109
[30] Ellis D J P, Stevenson R M, Young R J, Shields A J, Atkinson P and Ritchie D A 2007 *Appl. Phys. Lett.* **90** 011907